Available online at www.sciencedirect.com
ScienceDirect
Remote Sensing of Environment 107 (2007) 172–184
Remote Sensing of Environment
www.elsevier.com/locate/rse

Detection of daytime arctic clouds using MISR and MODIS data

Tao Shi [a,*], Eugene E. Clothiaux [b], Bin Yu [c], Amy J. Braverman [d], David N. Groff [e]

[a] Department of Statistics, The Ohio State University, Columbus, OH 43210-1247, United States
[b] Department of Meteorology, Pennsylvania State University, University Park, PA 16802, United States
[c] Department of Statistics, University of California, Berkeley, CA 94720-3860, United States
[d] Jet Propulsion Laboratory, California Institute of Technology, Pasadena, CA 91109-8099, United States
[e] Department of Energy, Southern Great Plains Site, 309600 EW 28, Billings, OK 74630, United States

Received 20 February 2006; received in revised form 12 October 2006; accepted 16 October 2006

Abstract

Expert labels were used to evaluate arctic cloud detection accuracies of several methods based on MISR angular radiances and MODIS spectral radiances. The accuracy of cloud detections was evaluated relative to 5.086 million expert labels applied to 7.114 million 1.1-km resolution pixels with valid radiances from 57 scenes. The accuracy of the MODIS operational cloud mask was 90.72% for the 32 partly cloudy scenes and 93.37% for the 25 completely clear and overcast scenes. An automated, simple threshold algorithm based on three features extracted from MISR radiances and the MODIS operational cloud mask agreed with each other for 74.91% of the pixels in the 32 partly cloudy scenes and 78.44% of the pixels in the 25 completely clear and overcast scenes. These subsets of pixels had, relative to the expert labels, classification accuracies of 96.53% for the 32 partly cloudy scenes and 99.05% for the 25 completely clear and overcast scenes. Fisher's quadratic discriminate analysis (QDA) trained on expert labels from the 32 partly cloud scenes was applied to MISR radiances, three features based on MISR radiances, MODIS radiances, and the six features of the MODIS operational cloud mask with accuracies ranging from 87.51% to 96.43%. Accuracies increased to about 97% when QDA with expert labels was applied to combined radiances or features from both MISR and MODIS. Operational QDA-based classifiers were developed using as training labels those pixels for which the MISR automated, simple threshold and MODIS operational cloud mask algorithms agreed. Training the QDA classifier on these automatic labels using MISR radiances, three features based on MISR radiances, MODIS radiances, and the six features of the MODIS operational cloud mask led to accuracies ranging from 85.23% to 93.62% for the 32 partly cloudy scenes. Classification accuracies increased to 93.74% (93.40%) when combined MISR and MODIS radiances (features) were used. The highest accuracy attained with any operational algorithm tested on all 57 scenes was 94.51%. These results suggest that both MISR and MODIS radiances are sufficient for cloud detection in daytime polar regions.

Keywords: Polar study; Cloud detection; MISR; MODIS

1. Introduction

Nadir radiances at different wavelengths (i.e., spectral radiances) across the shortwave and longwave electromagnetic spectra have served as the cornerstone of cloud detection from satellites from the advent of satellite meteorology (e.g., Rossow & Garder, 1993; Saunders & Kriebel, 1988; Stowe et al., 1999; Wielicki et al., 1996; Wielicki & Green, 1989). The launch of the Moderate Resolution Imaging Spectroradiometer (MODIS) onboard NASA's Earth Science Enterprise Terra and Aqua satellites represented the culmination of deliberate scientific planning to place on a single sensor all of the spectral channels necessary for global cloud detection. Amongst the 36 spectral channels available on the MODIS sensor six of them were chosen for detection of clouds in daytime polar regions (Ackerman et al., 2002; Table 1).

The value of spectral radiances for cloud detection has been investigated in detail, but the value of radiances emanating in different directions to space from the same object (i.e., angular radiances) has not (Diner et al., 1999). Studies of radiances from scenes simultaneously viewed by two geostationary satellites

* Corresponding author.
E-mail addresses: taoshi@stat.ohio-state.edu (T. Shi), cloth@meteo.psu.edu (E.E. Clothiaux), binyu@stat.berkeley.edu (B. Yu), Amy.Braverman@jpl.nasa.gov (A.J. Braverman), d_groff@ops.sgp.arm.gov (D.N. Groff).

0034-4257/$ - see front matter © 2006 Elsevier Inc. All rights reserved.
doi:10.1016/j.rse.2006.10.015

Table 1
The six MODIS nadir radiance band-center wavelengths, the six MODIS operational cloud mask algorithm features, the five MISR 0.620-μm radiance view zenith angles and the three MISR features used in this study

MODIS nadir radiance band-center wavelengths
0.865 μm (Band 2)
3.959 μm (Band 21)
1.375 μm (Band 26)
6.715 μm (Band 27)
11.030 μm (Band 31)
13.935 μm (Band 35)
MODIS spectral features
$I_{0.87,ij}$
$BT_{11.03,ij} - BT_{3.96,ij}$
$I_{1.38,ij}$
$BT_{6.72,ij}$
$BT_{11.03,ij} - BT_{6.72,ij}$
$BT_{13.94,ij}$
MISR 0.672-μm radiance view zenith angles
00.0° (AN Camera)
26.1° (AF Camera)
45.6° (BF Camera)
60.0° (CF Camera)
70.5° (DF Camera)
MISR Spatial and Angular Features
$LC_{ij} = \sum_{k=4i-5}^{4i+2} \sum_{l=4j-5}^{4j+2} (I_{f,kl} - \overline{I_{f,ij}})(I_{n,kl} - \overline{I_{n,ij}}) / \sqrt{\sigma_{f,ij}\sigma_{n,ij}}$
$\sigma_{n,ij} = \sqrt{\left(\frac{1}{64-1}\right) \sum_{k=4i-5}^{4i+2} \sum_{l=4j-5}^{4j+2} 37(I_{n,kl} - \overline{I_{n,ij}})^2}$
$NDAI_{ij} = (I_{f,ij} - I_{n,ij}) / (I_{f,ij} + I_{n,ij})$

The MODIS features consist of two radiances (I), two radiances converted to brightness temperatures (BT), and two radiances converted to brightness temperatures and differenced. The MISR features are linear correlations (LC) between small groups of radiances from two MISR view directions, one in the forward (f) direction and the other in the nadir (n) direction, standard deviations (σ) of small groups of radiances from the nadir view, and the normalized difference angular index (NDAI) based on comparing MISR nadir- and forward-view 0.620-μm radiances. The subscript pair ij indicates the pixel to which the features are attributed and $\bar{I}$ represents the average over the small groups of MISR radiances.

have been possible historically, but such investigations are not straightforward and are not easily extended to extensive data sets (Muller et al., 2002). The conical scanning patterns of the Along Track Scanning Radiometers, ATSR-1 on the ERS-1 satellite and ATSR-2 on the ERS-2 satellite, as well as the Advanced Along Track Scanning Radiometer (AATSR) on the ENVISAT satellite, have provided two different views of the same scene, which have proven useful in detecting clouds (Zavody et al., 2000). The Polarization and Directionality of the Earth's Reflectances (POLDER) radiometer–polarimeter launched on the Japanese ADEOS-I and ADEOS-II satellites provided information on cloud particle properties through coupled polarization and multi-directional measurements at up to 14 view directions (Parol et al., 2004).

The Multi-angle Imaging Spectroradiometer (MISR; Diner et al., 1998) launched with the MODIS sensor on the NASA Terra satellite measures the radiances from an object to space in nine different directions. Early investigations of images from each of the nine MISR view directions clearly indicated that angular radiances contained information on surface and cloud properties (e.g., Di Girolamo & Wilson, 2000; Nolin et al., 2002). Given that surface-leaving (scattered) radiances at visible wavelengths are more isotropic from surface snow and ice than they are from low-altitude, overcast, relatively smooth clouds, for which forward scattering is much greater than the other directions (Stephens et al., 1981), the results of these early investigations with MISR data were not unexpected. The NASA Terra satellite travels from north to south over the daylight side of the Earth, hence over the Arctic MISR forward-view camera radiances from clouds over snow- and ice-covered surfaces exceed those from the MISR nadir-view camera. Over Antarctica MISR's aft-view cameras record forward scattered radiation from clouds over snow- and ice-covered surfaces and these radiances exceed those from the MISR nadir camera. The directionality of the radiation scattered by clouds and snow- and ice-covered surfaces and recorded by MISR is one feature that we use in the current study.

To make maximum use of MISR's nine angular radiances for science applications, MISR operational processing registers the radiances from each of its nine view directions to the exact same (space-oblique mercator) grid of points on an ellipsoid surface (the World Geodetic System 1984, or WGS84, ellipsoid surface) at sea level and underlying terrain (Jovanovic et al., 2002, 1998). In one registration approach, the ellipsoid projection approach, terrain is neglected and the radiances are projected and re-sampled directly to the space-oblique mercator grid of points on the ellipsoid surface (Fig. 1). In the second approach the radiances are first projected to the terrain and then re-sampled to space-oblique mercator grid points on the ellipsoid surface underlying the terrain (Fig. 1). Each time MISR orbits over one of its 233 distinct paths relative to the surface, the nine sets of MISR camera radiances are registered to the exact same grid point locations as for all of the past, as well as future, MISR orbits over this path. If the registration was perfect, and the illumination, surface and atmosphere the same, for two orbits of MISR over the same surface location (i.e., the same path) the two images for each MISR view direction would be identical. This operational registration process, more formally called georectification, allows for a second unique feature to be produced by MISR for detection of clouds.

In this study six spectral radiances from MODIS and six features based on them are co-registered with five angular radiances from MISR and three features extracted from them (Table 1). Combinations of MISR and MODIS radiances and features, in conjunction with training labels of clear and cloudy pixels, are used to train Fisher's quadratic discriminate analysis (QDA) classifiers. Performances of the QDA classifiers in separating clear from cloudy pixels are subsequently compared with MODIS operational cloud mask results and the accuracies of all classifiers are assessed with expert labels.

2. Methods

The accuracies of cloud detections based on MISR angular radiances and features, MODIS spectral radiances and features,

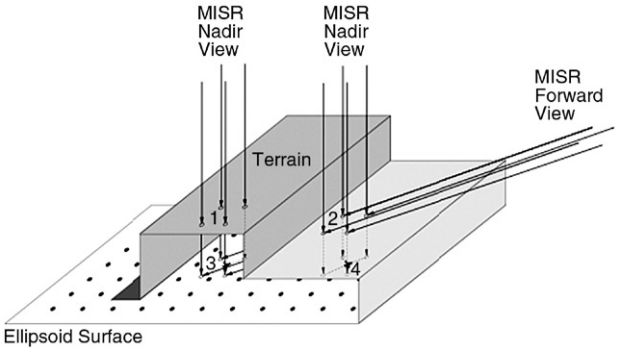

Fig. 1. Cartoon illustration of MISR space-oblique mercator grid point locations (solid dots) on the reference ellipsoid surface. In the ellipsoid projection terrain zenith radiances from location 1 that contribute to the MISR nadir view and terrain 70.5° forward scattered radiances from location 2 that contribute to the MISR forward view are mapped to the same grid location at 3. In the terrain projection terrain zenith radiances from location 2 that contribute to the MISR nadir view and terrain 70.5° forward scattered radiances from location 2 that contribute to the MISR forward view are mapped to the same grid location at 4. In the absence of clouds the nine MISR radiances from a specific surface feature have the same grid point location in the terrain projection but they have different grid point locations in the ellipsoid projection. As a surface feature lies closer to the ellipsoid surface containing the grid points, the differences in the locations of the nine MISR radiances from the surface feature in the ellipsoid projection become smaller. The nine MISR radiances from a cloud above the terrain are mapped to different grid point locations in both the ellipsoid and terrain projections.

and combinations of them are evaluated relative to 2.685 million expert labels applied to 3.946 million valid sets of 1.1-km resolution radiances from 32 partly cloudy scenes and 2.401 million expert labels applied to 3.168 million valid sets of 1.1-km resolution radiances from 27 completely clear and overcast scenes. The 7.114 million valid sets of radiances are from 10 orbits of Terra path 26 over the Arctic Ocean, northern Greenland and Baffin Bay (Fig. 2). The repeat time between two consecutive orbits over the same path is 16 days, so the 10 orbits span 144 days from April 28 through September 19, 2002. Path 26 was chosen for the study because of the richness of its surface features, which include permanent sea ice in the Arctic Ocean, snow-covered and snow-free coastal mountains in Greenland, permanent glacial snow and ice, and sea ice that melted across Baffin Bay over the 144 days.

Seven MODIS radiance images for the third scene from the top of Fig. 2, with icebergs, open water, and coastal hills, are illustrated in Fig. 3a–g. Comparing MODIS radiances in Fig. 3a–g with expert labels of clear and cloudy pixels in Fig. 3h, each set of radiances is seen to characterize different aspects of the surface and cloud objects across the scene. Ackerman et al. (2002) clearly describe the value of MODIS radiances for detecting clouds. To develop single-value thresholds that best separate clear from cloudy pixels, transformation of radiances for a pixel is often useful. The MODIS operational cloud mask algorithm makes use of six features for daytime polar regions (Ackerman et al., 2002). As Table 1 illustrates, two of the MODIS features are radiances, two are radiances transformed to brightness temperatures, and two are radiances transformed to brightness temperatures and then differenced.

The scene presented in Fig. 3 with MODIS spectral radiances is illustrated in Fig. 4 with MISR 0.672 μm nadir and 70.5° forward-view radiances. The MISR 70.5° forward-view (forward-scattered) radiances are distinctly different from the nadir spectral radiances for cloudy scenes. It is these differences between the nadir- and forward-view radiances for clear and cloudy scenes that make the forward-view radiances of value for cloud detection in the Arctic.

2.1. MISR and MODIS data

The four spectral (i.e., 0.446 μm, 0.558 μm, 0.672 μm, 0.866 μm) radiances available from each of the nine MISR cameras are similar to four of those on MODIS. These four spectral radiances do not contain significantly different information of clouds over snow and ice surfaces. Only the MISR 0.672 μm (red) radiances have 275-m resolution in all nine MISR cameras, with the other three spectral radiances having 1.1-km resolution in the off-nadir cameras. For these reasons we used only MISR 0.672 μm (red) radiances in this study. An earlier study by Nolin et al. (2002), together with our own inspection of MISR imagery, led us to conclude that most of the

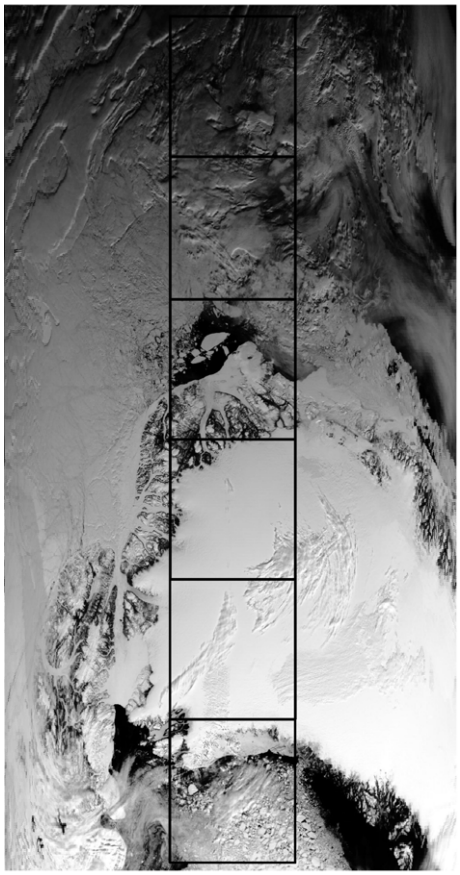

Fig. 2. MODIS 0.659-μm radiance image of the Arctic Ocean, northern Greenland, and Baffin Bay on May 30, 2002. White represents large radiance values and black represents low radiance values. Black boxes within the image show the approximate locations of consecutive three-block groups of MISR nadir radiances (i.e., a scene of radiances) obtained at the same time as the MODIS radiances.

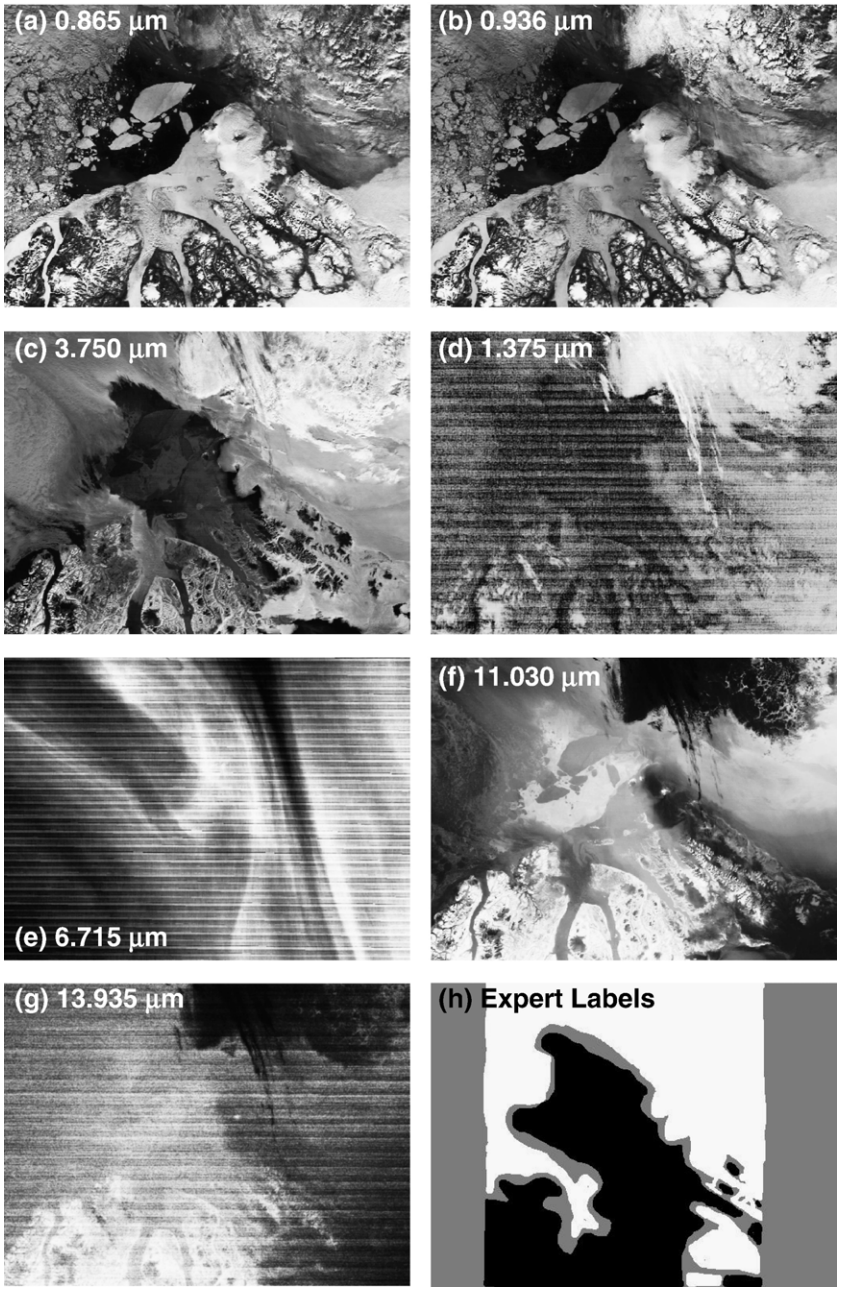

Fig. 3. MODIS a) 0.865 μm, b) 0.936 μm, c) 3.750 μm, d) 1.375 μm, e) 6.715 μm, f) 11.030 μm, and g) 13.935 μm radiance images for the third (from top) three-block MISR scene illustrated in Fig. 2. The scene contains icebergs, open water, coastal hills, and a variety of cloud types. The radiances in a)–g) have been histogram-equalized for contrast enhancement with white representing large radiance values and black small radiance values. h) Expert labels of clear (black) and cloudy (white) pixels for the scene together with pixels that were not labelled (grey).

information of arctic clouds is contained in the radiances from the MISR nadir and forward views, hence we used radiances only from the MISR nadir and four forward-view cameras. The MODIS radiances are of 1-km resolution and the expert labels of 1.1-km resolution, hence we used MISR red radiances and features of nominal 1.1-km resolution that were constructed from the 275-m resolution red radiances.

For this study we used MISR ellipsoid-projected red radiances for ocean scenes and terrain-projected red radiances for land scenes. Terrain-projected radiances are available only for land locations specified by the land mask implicit within the terrain-projected radiance data set (Jovanovic et al., 1998). Identification of ellipsoid-projected radiances over ocean is accomplished by noting those locations for which the terrain-projected radiances do not exist. We used the MISR red radiances in the space-oblique mercator projection in which they come. Images of MISR data in Fig. 4 are for the data in their native space-oblique mercator projection.

We investigated classification accuracies of the MODIS operational cloud mask algorithm and of classifiers trained with MODIS radiances and features based on these radiances. For this reason both MODIS radiance and cloud mask files were

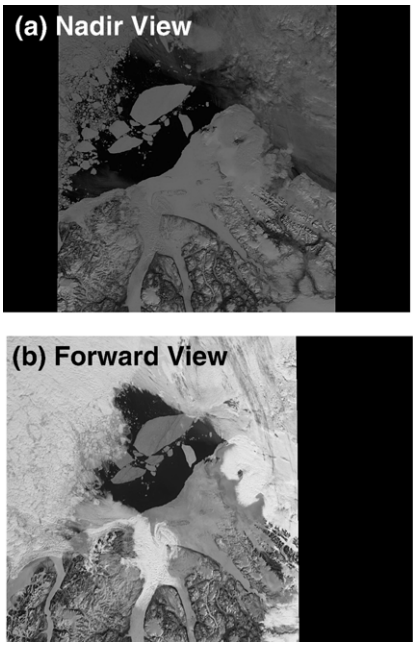

Fig. 4. MISR a) nadir and b) 70.5° forward view radiance images for the third (from top) three-block MISR scene illustrated in Fig. 2. The radiances in the two images are presented on the same linear scale for comparative purposes, with white representing large radiance values and black small radiance values.

necessary. All 36 1-km resolution radiances were extracted from collection 4 MOD021KM files, whereas the 1-km resolution cloud mask results were extracted from collection 4 MOD35_L2 files.

The 36 spectral radiances and cloud mask results for each pixel, together with the pixel latitude and longitude, were extracted from the MODIS files. The latitudes and longitudes of MODIS pixels were subsequently used to project the MODIS 1-km resolution radiances and cloud mask results into the 1.1-km resolution space-oblique mercator projection of the MISR data. A nearest-neighbor algorithm assigned one set of projected MODIS pixel values to each MISR space-oblique mercator grid point location. Images of MODIS data in Fig. 3 are for MODIS data in MISR's space-oblique mercator projection.

In the last step MISR and MODIS radiances were transformed into the three MISR and six MODIS operational features for cloud detection in daytime polar regions. The MODIS radiances and features, which are of 1-km resolution, are reported on the 1.1-km MISR grid. The MISR 275-m resolution angular red radiances are used in groups of 8 by 8, i.e., 2.2 km by 2.2 km, to compute the MISR spatial linear correlation and standard deviation features with the results reported on the 1.1-km MISR grid. The 275-m resolution angular red radiances were then averaged to 1.1-km resolution for computation of the third MISR feature, called the normalized difference angular index (NDAI). That is, all three MISR features are reported on the 1.1-km MISR grid with two of them of 2.2-km resolution and the other of 1.1-km resolution.

The MISR and MODIS radiance and feature data were divided into scenes composed of three of MISR's 180 blocks along the Terra satellite orbit (black boxes in Fig. 2). Each three-block scene of MISR and MODIS data consists of approximately 384 across track by 384 along track useable pixels, all with 1.1-km grid spacing. With 57 scenes of 384 by 384 useable pixels per scene we would expect to have 8.405 million pixels for this study. However, we have only 7.114 million pixels. The difference is a result of the MISR nadir and four forward-view blocks of 384 by 384 radiances not perfectly overlapping with each other. An example of the offsets between images from the different MISR camera views is shown in Fig. 4, in which the forward-view camera image is offset to the west of the nadir-view camera image.

2.2. The expert labels

For each three-block scene images of the MODIS spectral radiances useful for cloud detection, i.e., Bands 1–7, 17–23, 26–29, and 31–35, were cataloged into a file in which switching between images was relatively easy. Images of the nine MISR ellipsoid-projected red radiance data sets were made into an animated movie that enabled scanning through the nine images, starting from the DF (forward-view) camera image and ending with the DA (aft-view) camera image. The labelling process started with inspection of the MISR movie played at varying scan rates. The apparent motions in the MISR movies of clouds, shadows and high altitude land that result from changing projection locations from one camera to the next are a powerful method for manual cloud detection. This process, coupled with inspection of the MODIS radiances as necessary, enabled unambiguous identification of optically thin clouds over any surface and optically thick clouds over bright, white surfaces, such as glacial ice flows in the valleys of the coastal mountains of Greenland. Software image analysis tools were subsequently used to label the pixels in MISR nadir camera images as clear or cloudy.

Our subjective impression was that the MISR and MODIS radiances were sufficient by themselves to label as clear or cloudy all of the pixels in each three-block scene. To do so, however, would take an inordinate amount of time. Most of the arctic clouds in the 10 orbits processed for this study were laminar in nature. In the labelling process the cores of clear and cloudy regions were labelled, usually up to, but not including, cloud edges. Labels were applied throughout each scene in order to sample a range of illumination and view geometries for a large variety of surface types. We labelled 2.685 million of the 3.946 million pixels (i.e., 68%) from the 32 partly cloudy scenes and 2.401 million of the 3.168 million pixels (i.e., 76%) from the 25 completely clear and overcast scenes.

The goal of our labelling process was to provide accurate identification of clear and cloudy pixels, where a clear pixel was free of any cloud and a cloudy pixel contained at least some cloud. By labelling the cores of clear and cloudy regions, and avoiding their edges, we most likely labelled only completely clear and cloud overcast pixels. This expectation is a reasonable one to us given that broken, sub-pixel (less than 1-km in lateral extent) clouds were not prevalent in our study. The lack of small cloud elements and the occurrence of clear and cloudy areas over large spatial scales limits the deleterious impact of sub-pixel cloudiness and cloud edges on our results.

The drawbacks of our approach are two-fold. By not labelling the edges of clear and cloudy regions we may limit the extent of labelled data in the space of radiances and features in which the classifiers operate, with the result that the classifier boundaries may not be optimally positioned. A second drawback is that we cannot evaluate classifier performance near cloud edges, which contain pixels that may be difficult to classify as clear or cloudy. As a result, the classification accuracies that we report are upper bounds on the performance of the classifiers tested in this study and actual performances for all pixels in a scene will be less by some unknown amount. This is true of the Fisher's quadratic analysis (QDA) classifier results, as it is for the MODIS operational cloud mask algorithm results.

Assessing quantitatively the performance of any MISR or MODIS cloud mask algorithm near cloud edges is difficult at best. Ground-based data from active sensing systems are too sparse to assess rigorously such algorithms over regional to global spatial scales. The Advanced Spaceborne Thermal Emission and Reflection Radiometer (ASTER) has high spatial resolution, making it suitable for studying sub-pixel optically thick clouds within MISR and MODIS pixels, but it lacks the richness of spectral and angular information that MISR and MODIS have for detecting optically thin clouds over snow and ice surfaces. The best data for assessing the performance of the classifiers would be space-based lidar data coincident with MISR and MODIS data, but such data do not exist.

2.3. The three MISR features

The three MISR features (Table 1; Shi et al., 2004) for this study require radiances originating from land- and sea-ice surfaces to have the same grid point locations in the images from the five MISR cameras used in the study. Therefore, for ocean scenes with sea ice we used MISR ellipsoid-projected radiances and for land terrain-projected radiances. With this choice radiances from all MISR cameras that originate from the same land or sea ice surface have an identical grid point location in the images. This attribute of MISR radiances allows for unique cloud detection features.

If a cloud is above the underlying ocean or land surface, the radiances associated with the cloud will have different locations in the ellipsoid- and terrain-projected images for all MISR cameras. Now assume that the spatial pattern of radiances associated with a surface or cloud object is similar for the five MISR camera views. Further assume that the spatial patterns of radiances from two different clouds, or different parts of the same cloud, have no correlation with each other between any two MISR views. If these assumptions are valid, which they appear to be, the spatial correlation of radiances from the same grid locations between any two MISR views will be high for clear (cloud-free) oceanic regions in the ellipsoid-projected images and land-surface regions in the terrain-projected images. The spatial correlation will be low when clouds above the ocean or land surface obscure either one or both of any two MISR views.

The feature that we used to test the spatial correlation of radiances from the same grid point locations between two different views is the linear correlation (LC) of eight by eight groups of 275-m resolution MISR red radiances centered on one 1.1-km grid point location indexed by (i, j):

$$LC_{ij} = \frac{\sum_{k=4i-5}^{4i+2}\sum_{l=4j-5}^{4j+2}(I_{\mathrm{f},kl}-\overline{I_{\mathrm{f},ij}})(I_{\mathrm{n},kl}-\overline{I_{\mathrm{n},ij}})}{\sqrt{\sigma_{\mathrm{f},ij}\sigma_{\mathrm{n},ij}}}, \quad (1)$$

where $I_{\mathrm{f},kl}$ and $I_{\mathrm{n},kl}$ are the MISR forward- and nadir-view 275-m resolution radiances at location (k, l), $\overline{I_{\mathrm{f},ij}}$ and $\sigma_{\mathrm{f},ij}$ are the mean and standard deviation of the 64 forward-view radiances associated with location (i, j), and $\overline{I_{\mathrm{n},ij}}$ and $\sigma_{\mathrm{n},ij}$ are similarly defined for the nadir-view radiances. The linear correlation is computed from 64 275-m resolution radiances covering 2.2 km by 2.2 km of area and is attributed to the 1.1 km by 1.1 km area at the center of the 2.2 km by 2.2 km area in order to match the spatial resolution of the expert labels and MODIS data. The choice of 64 radiances was a trade-off between restricting the linear correlation to a small area and having sufficient statistics to reliably compute the linear correlation. The means are arithmetic averages and the standard deviations are given by

$$\sigma_{\mathrm{fn},ij} = \sqrt{\left(\frac{1}{64-1}\right)\sum_{k=4i-5}^{4i+2}\sum_{l=4j-5}^{4j+2}(I_{\mathrm{fn},kl}-\overline{I_{\mathrm{fn},ij}})^2}. \quad (2)$$

The linear correlation feature is assumed to return a high value for surface objects and a low value for clouds. Locally (i.e., 2.2 km by 2.2 km) smooth surface objects, in this study always glacial ice and snow regions, and extremely low (less than 500 m) altitude clouds and fog are problematic. For locally smooth surface objects the spatial variations of nadir- and forward-view radiances are sufficiently small that the linear correlations between the two views are low. To test for locally smooth surface features the standard deviation ($\sigma_{\mathrm{n},ij}$) of the nadir-view radiances over eight by eight 275-m resolution radiances is a useful feature.

Exploratory data analysis indicated that the MISR 70.5° forward view was not best for cloud detection using linear correlations between MISR camera pairs, hence we used MISR camera views closer to nadir. We computed linear correlations between MISR nadir and 26.1° forward view and MISR nadir and 45.6° forward view red radiances and averaged the two results to obtain the linear correlation feature.

The third, and final, MISR cloud detection feature is motivated by Fig. 4. Surface-leaving (scattered) radiances at visible wavelengths are more isotropic from surface snow and ice than they are from low-altitude, overcast, relatively smooth clouds for which forward scattering dominates. As such, the differences between radiances from the nadir- and forward-view MISR cameras are useful for low-altitude cloud detection over Arctic snow- and ice-covered surfaces. (Note that forward scattering of radiation from clouds over Antarctica is recorded

by the aft-view MISR cameras.) This finding motivates use of the ratio

$$\mathrm{NDAI}_{ij} = \frac{I_{\mathrm{f},ij} - I_{\mathrm{n},ij}}{I_{\mathrm{f},ij} + I_{\mathrm{n},ij}}, \tag{3}$$

called the normalized difference angular index (NDAI; Nolin et al., 2002), as the third feature. The radiances in NDAI have 1.1-km resolution, similar to the spatial resolution of the MODIS radiances and features, and are obtained by averaging 16 275-m resolution red radiances over a 1.1 km by 1.1 km area. In the current implementation over the Arctic the MISR 70.5° forward-view radiance, i.e., the most forward-scattered radiance recorded by MISR, is compared with the radiance from the nadir camera.

2.4. Classifiers for MISR and MODIS radiances and features

To label automatically radiances as cloudy or clear (i.e., cloud free) using the five angular MISR radiances, the three MISR features, the six MODIS radiances, and the six MODIS features, Fisher's quadratic discriminate analysis (QDA), which requires training labels, is employed. For one set of experiments training labels are from the expert labels and in a second set from those pixels for which results from the MODIS operational cloud mask and a second automated algorithm applied to the three MISR features agree. Results from the first set of experiments represent the best possible in our current set-up, whereas the second set of experiments represent automatic labelling schemes to be used operationally for cloud mask generation. Performances of the QDA classifiers in separating clear from cloudy pixels are always assessed with expert labels. In training of the classifiers with expert labels only half of the expert labels (chosen at random) are used and the remaining half is withheld for testing. All of the expert labels are used to assess the performances of the automated algorithms.

Single-value threshold labelling methods, i.e., single-value thresholds applied separately to each feature and reduced to a single clear/cloudy classification using a decision tree, are evaluated relative to the expert- and automatic-trained QDA classifier results. To make the study relevant to MODIS operational processing MODIS cloud mask results were used directly rather than developing independent single-value thresholds to be applied to each MODIS feature. The rationale for the MODIS single-value thresholds and decision tree (i.e., the MODIS operational cloud mask algorithm) is described by Ackerman et al. (1998, 2002) and is not reproduced here.

2.4.1. MISR single-value thresholds

Stable and robust thresholds for the linear correlation (LC_{ij}) and standard deviation ($\sigma_{\mathrm{n},ij}$) were found by analyzing sets of the three MISR features from a variety of scenes across different orbits and visually inspecting clear and cloudy pixel classification results obtained from them. For this study the empirically determined threshold t_{LC} on LC_{ij} was set to 0.75 and the threshold t_σ on $\sigma_{\mathrm{n},ij}$ was set to 2. The appropriate threshold t_{NDAI} for NDAI_{ij} changed from scene to scene. On a scene-by-scene basis NDAI_{ij} is a useful feature for separating clear and cloudy pixels but the threshold that separates the two classes is, unfortunately, scene dependent. We must have an automated method for estimating the best threshold t_{NDAI} for each scene.

The method adopted to set t_{NDAI} was based on modelling NDAI_{ij} values for three-block scenes as a mixture of two Gaussian distributions, one for the cloudy pixels and the other for the clear pixels. The choice of two Gaussian distributions to model NDAI_{ij} values was made for two reasons. Two Gaussian distributions fit the three-block frequency of occurrence histograms of NDAI_{ij} well and the computation of mixed Gaussian fits to NDAI values is relatively straightforward. Three blocks of MISR data were modelled together, representing a compromise between ensuring both cloudy and clear areas within the region and separability of NDAI_{ij} values for cloudy and clear areas. Modelling more than three MISR blocks of data together provides a greater probability of having both clear and cloudy pixels. However, histograms of NDAI_{ij} for cloudy and clear areas in an extended block range often broaden, leading to poorer separability.

The minimum, or dip, between the peaks of the two Gaussian distributions was taken as t_{NDAI}, assuming, of course, that there was a minimum in the distribution. Manually analyzing several three-block scenes we found that the minima between the peaks of the two Gaussian distributions, and hence t_{NDAI}, generally fell between 0.08 and 0.40. If no minimum was found between the peaks of the two Gaussian distributions or there was a minimum but it was outside the empirically determined expected range from 0.08 to 0.40, the threshold from either the previous orbit or the next orbit was selected if one of the two was available. If neither of these two thresholds existed, the average of all available thresholds for this three-block scene over all 10 orbits was used.

The decision tree for reducing the three MISR features to a single clear/cloud classification, called the MISR Enhanced Linear Correlation Matching (ELCM) algorithm, is straightforward (Shi et al., 2004). The 1.1-km by 1.1-km resolution pixel (i, j) is classified as clear if $\sigma_{\mathrm{n},ij} < t_\sigma$ or if $\mathrm{LC}_{ij} > t_{\mathrm{LC}}$ and $\mathrm{NDAI}_{ij} < t_{\mathrm{NDAI}}$. When this test fails, the region is labeled as cloudy.

2.4.2. Quadratic discriminate analysis classifier

Single-value thresholds divide a multi-dimensional feature space into rectangular regions. However, the boundary between clear and cloudy pixels may be nonlinear and may not particularly follow any one of the three coordinate axes (Shi, 2005). Fisher's quadratic discriminate analysis supplies a quadratic classification boundary that is expected to be more accurate than single-value thresholds applied to each feature separately. Implementation of quadratic discriminate analysis requires training data to construct the boundaries (e.g., Mardia et al., 1979; Ripley, 1996).

In a two class (i.e., clear and cloudy) classification problem, quadratic discriminate analysis models each class probability density as a multivariate Gaussian distribution:

$$f_k(x) = \frac{1}{(2\pi)^{p/2}|\sum_k|^{1/2}} e^{-\frac{1}{2}(x-\mu_k)^T \sum_k^{-1}(x-\mu_k)}, \tag{4}$$

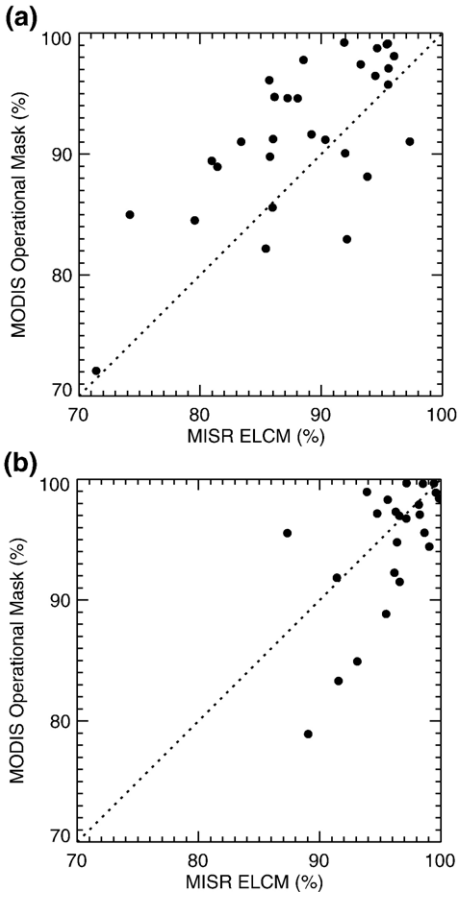

Fig. 5. Percentage of MODIS operational cloud mask versus MISR ELCM algorithm classifications that are correct relative to expert labels for a) the 32 partly cloudy scenes and b) the 25 completely clear and overcast scenes.

where $k=1, 2$ denotes the class label (i.e., clear or cloudy), $f_k(x)$ is the probability density function of the multi-dimensional feature vector x belonging to class k, p is the dimension of x, μ_k – a multi-dimensional vector – is the population mean of the multi-dimensional feature vectors, and $\sum_k$ – a multi-dimensional square matrix – is the population variance amongst the feature vectors. Let π_k be the prior probability of class k, which is simply the probability of class k in the training data. An a posterior distribution for x belonging to class k is then given by

$$P(x\in\text{Class } k|X=x)=\frac{f_k(x)\pi_k}{f_1(x)\pi_1+f_2(x)\pi_2}. \quad (5)$$

The classification rule of quadratic discriminate analysis is to place x in the class that has the largest a posterior probability for x.

In summary, the parameters π_k, μ_k, and $\sum_k$ are estimated by the empirical class proportions, means, and variances in the training data and subsequently substituted into the above two equations to form the classifier. Eq. (5) for a novel feature vector x is evaluated for the clear and cloudy classes and the novel feature vector is assigned to the class with the highest probability.

2.4.3. Radiance- and feature-based classification tests

As a test of the value of MODIS and MISR radiances for cloud detection quadratic discriminant analysis classifiers were trained

Table 2
Classification accuracies and scene coverages of the three operational classifiers for all 57 scenes, the 32 partly cloudy scenes, and the 25 completely clear and overcast scenes

	Number	MISR ELCM	MODIS operational	Agreed
All scenes	57	91.80%	91.97%	97.75%
Coverage		100.00%	100.00%	76.58%
Land		90.32%	90.71%	98.50%
Ocean		92.33%	92.40%	97.41%
Partly cloudy	32	88.63%	90.72%	96.53%
Coverage		100.00%	100.00%	74.91%
Land		88.10%	88.47%	96.46%
Ocean		88.93%	91.34%	95.01%
Clear/overcast	25	95.39%	93.37%	99.05%
Coverage		100.00%	100.00%	78.44%
Land		94.44%	95.05%	99.25%
Ocean		95.48%	92.59%	98.76%

Scene coverages are given as percentages of all pixels in the study and the accuracy rates are for the subset of pixels for which expert labels are also provided. The operational classifiers are the MISR ELCM algorithm, the MODIS operational cloud mask algorithm, and those pixels for which the MISR ELCM and MODIS operational cloud mask algorithms agreed. Ocean results are for Baffin Bay and the Arctic Ocean north and east of Greenland. The land results are primarily from northern Greenland.

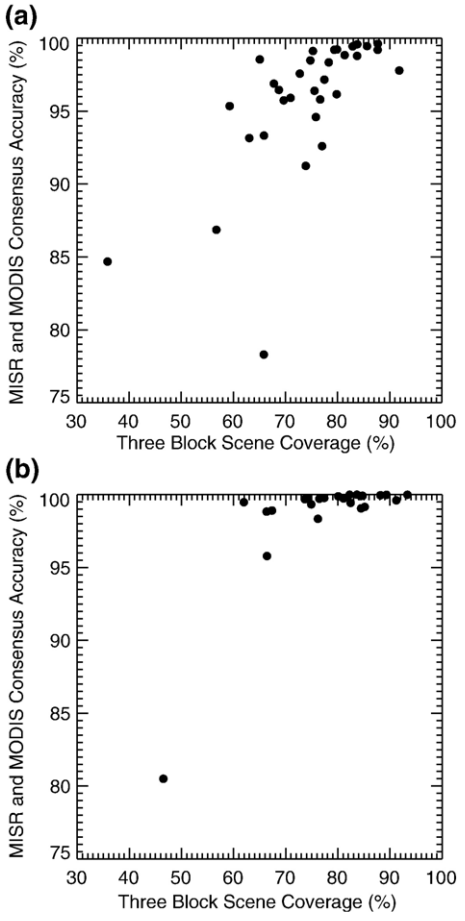

Fig. 6. Percentage of correct classifications relative to the expert labels of those pixels for which the MODIS operational cloud mask and MISR ELCM algorithms agreed versus the three-block scene coverage (i.e., percent of pixels in the three-block scenes which were in agreement) for a) the 32 partly cloudy scenes and b) the 25 completely clear and overcast scenes.

on half the expert labels using the five MISR radiances from the nadir and four forward-view cameras, the three MISR features, the six MODIS radiances for daytime cloud detection in polar regions, the six MODIS features, the five MISR angular radiances combined with the six MODIS spectral radiances, and the three MISR features combined with the six MODIS features as the classifier feature vectors. These six classifiers were subsequently tested on the remaining half of the expert labels to assess the value of MISR and MODIS radiances for cloud detection. To assess the effectiveness of single-value threshold classifiers the MODIS operational cloud mask results are evaluated relative to all of the expert labels, as are results from the MISR ELCM algorithm.

In the last classification test an attempt is made to develop an automated algorithm that improves upon the results from the

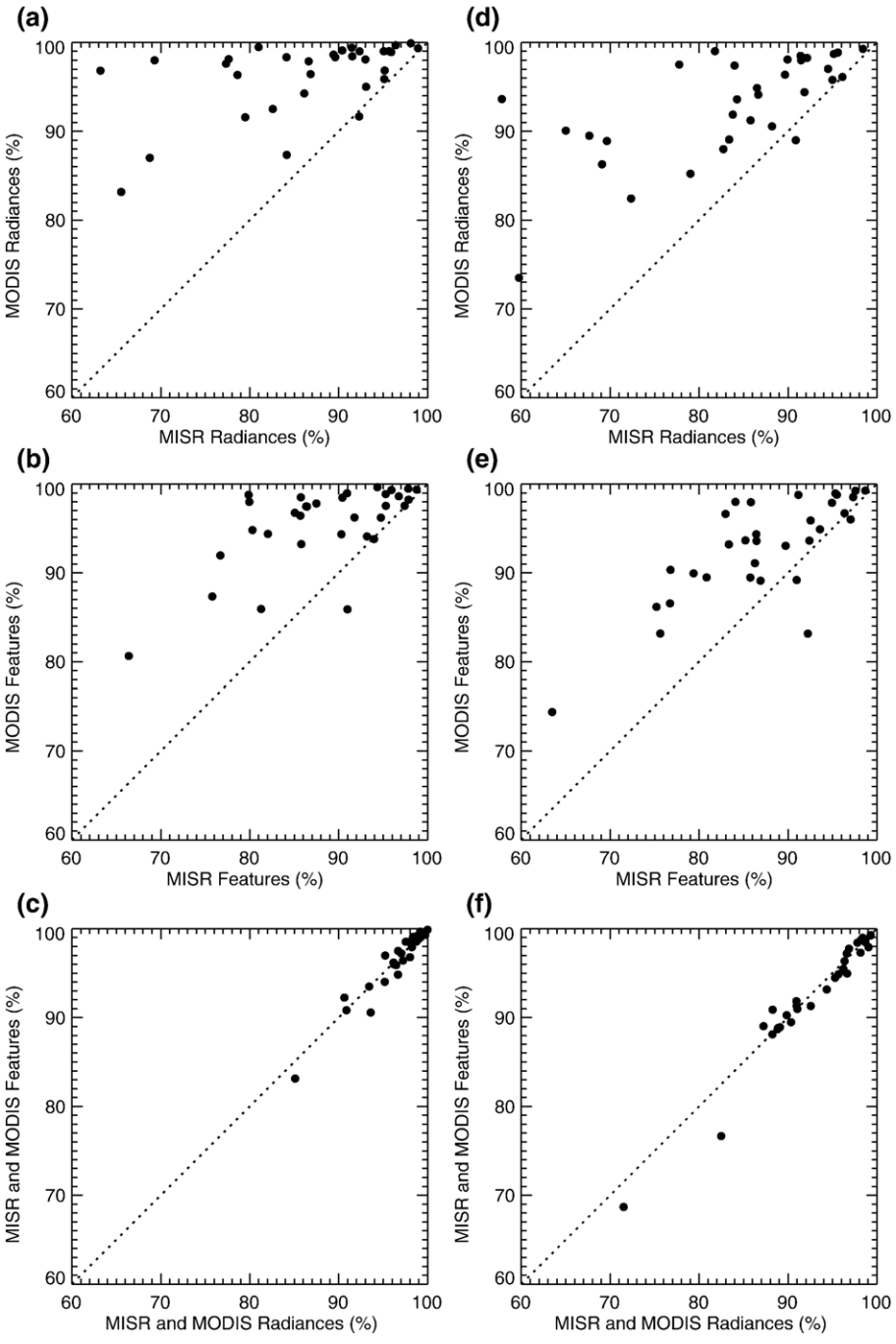

Fig. 7. Percentage of MODIS- and/or MISR-based classifications that are correct relative to one-half of the expert labels for a quadratic discriminant analysis classifier trained on the other half of expert labels using a) either five MISR or six MODIS radiances as input to the classifier, b) either three MISR or six MODIS features as input to the classifier, and c) either combined MISR and MODIS radiances or features as input to the classifier. Percentage of MODIS- and/or MISR-based classifications that are correct relative to all of the expert labels for a quadratic discriminant analysis classifier trained on those pixels for which the MISR ELCM and MODIS operational cloud mask algorithms agreed using d) either five MISR or six MODIS radiances as input to the classifier, e) either three MISR or six MODIS features as input to the classifier, and f) either combined MISR and MODIS radiances or features as input to the classifier.

Table 3
Classification accuracies (with 100% scene coverages) of QDA classifiers trained on expert labels, those pixels for which the MODIS operational cloud mask and MISR ELCM algorithms agreed, and only the MODIS operational cloud mask results

Training labels	MISR-R	MISR-F	MODIS-R	MODIS-F	All-R	All-F
Expert labels	87.51%	88.45%	96.43%	95.98%	96.98%	96.99%
Land	87.25%	88.41%	96.43%	96.93%	97.49%	97.66%
Ocean	88.22%	88.54%	96.43%	93.44%	95.59%	95.27%
Agreed pixels	85.23%	88.05%	93.62%	93.61%	93.74%	93.39%
Land	84.97%	87.94%	93.57%	94.36%	94.26%	93.91%
Ocean	85.95%	88.35%	93.72%	91.64%	92.32%	92.07%
MODIS mask	NA	NA	89.02%	88.88%	NA	NA
Land	NA	NA	88.93%	91.33%	NA	NA
Ocean	NA	NA	89.40%	83.00%	NA	NA

The QDA-based input feature vectors are the five MISR radiances (MISR-R), the three MISR features (MISR-F), the six MODIS radiances (MODIS-R), the six MODIS features (MODIS-F), the five MISR and six MODIS radiances (All-R), and the three MISR and six MODIS features (All-F). Ocean results are for Baffin Bay and the Arctic Ocean north and east of Greenland. The land results are primarily from northern Greenland.

single-value threshold algorithms applied separately to MISR and MODIS data. The approach adopted here treats as training data those pixels for which the MODIS operational cloud mask and MISR ELCM algorithms agree. These automatically generated training data, which cover only a subset of pixels in a scene, were then used to train one quadratic discriminant analysis classifier based on the five MISR and six MODIS radiances and a second classifier based on the three MISR and six MODIS features. Once the quadratic discriminant analysis classifiers were trained using the automatic labels, they were used to classify all of the pixels in a scene as either clear or cloudy and their performances were evaluated using all of the expert labels.

3. Results

Classification accuracies, relative to the expert labels, of the MISR ELCM and MODIS operational cloud mask (single-value threshold) algorithms are illustrated in Fig. 5 and Table 2. For the 32 partly cloudy scenes classification accuracies of these two algorithms were 88.63% and 90.72%. For the 25 completely clear and overcast scenes the accuracy of the two algorithms increased to 95.39% and 93.37%. For all 57 scenes classification accuracies of these two algorithms were 91.80% and 91.97%. We separated these results, as well as the others that follow, into those for land, primarily northern Greenland, and ocean, primarily Baffin Bay and the Arctic Ocean north and east of Greenland. We found that classification accuracies for land and ocean scenes were similar, which is not unexpected given that they are both primarily snow- and ice-covered, precluding the need to discuss them separately.

The subset of MISR ELCM and MODIS operational cloud mask results that agree with each other have classification accuracies, relative to the expert labels, of 96.53% and 99.05% for the 32 partly cloudy and 25 completely clear and overcast scenes (Fig. 6; Table 2). This subset of pixels covers 74.91% of the partly cloudy scenes and 78.44% of the completely clear and overcast scenes. These results suggest that this subset of pixels, which is generated by two automated cloud detection algorithms, may be suitable for training a quadratic discriminant analysis classifier for each scene, which in turn may lead to high classification accuracies with 100% coverage.

The value of MISR and MODIS radiances for cloud detection is next quantified relative to expert labels using a quadratic discriminant analysis classifier. The quadratic discriminant analysis classifier is trained using one half of the 2.685 million 1.1-km resolution expert labels from the 32 partly cloudy scenes. For this classifier training is equivalent to computation of π_k, μ_k, and $\sum_k$ in Eq. (4) using the different sets of input data — MISR angular radiances, MISR features, MODIS spectral radiances, MODIS features, MISR angular radiances combined with MODIS spectral radiances and MISR features combined with MODIS features. Once the classifier was trained with clear and cloudy pixels from scenes with both, the two-class (i.e., clear and cloudy) probabilities were computed via Eq. (5) for the remaining half of the pixels with expert labels and used to classify each pixel as either clear or cloudy. The percentage of correct classifications relative to the expert labels was then computed.

Fig. 7a–c illustrates scene-by-scene results from this analysis. Overall, the MISR radiance (MISR-R), MISR feature (MISR-F), MODIS radiance (MODIS-R), and MODIS feature (MODIS-F) classifiers were found to be correct for 87.51%, 88.45%, 96.43%, and 95.98% of the expert labels (Table 3). For combined MODIS and MISR radiances (All-R) the classification accuracy was 96.98% (Table 3). For combined MODIS and MISR features (All-F) the classification accuracy was 96.99%. For the current analysis approach these results represent the best possible and are the ones against which other classification methods are compared.

Quadratic discriminant analysis classifiers cannot be trained on scenes with pixels of only one type (i.e., clear or cloudy) because implicit in the approach is a two-class model. For completely clear and overcast scenes values for π_k, μ_k, and $\sum_k$ obtained from other partly cloudy scenes were used. Extracting values for these three parameters from the locations of the completely clear and overcast scenes, but from orbits that occurred 16 days prior to the completely clear and overcast

Table 4
Comparisons (in percent agreement) of the MISR ELCM, MODIS operational and quadratic discriminant analysis (QDA) classifiers (trained on those pixels for which the MISR ELCM and MODIS operational cloud mask algorithms agreed) when applied to the (68%) labeled and (32%) unlabeled pixels from the 32 partly cloudy scenes

	Labeled pixels	Unlabeled pixels
MISR ELCM/MODIS operational	87.77% (58.06%)	71.15% (77.27%)
All-R/MISR ELCM	87.76% (39.28%)	68.11% (22.89%)
All-R/MODIS operational	91.97% (41.93%)	82.92% (53.28%)
All-F/MISR ELCM	80.14% (19.49%)	67.16% (18.84%)
All-F/MODIS operational	83.08% (19.62%)	79.79% (44.95%)

The QDA-based input vectors are the five MISR and six MODIS radiances (All-R) and the three MISR and six MODIS features (All-F). The numbers in parentheses are the percent of those pixels in disagreement that are labeled as cloudy by the algorithm listed first in the left column and clear by the algorithm listed second.

Table 5
Of the expertly labeled cloudy and clear pixels in disagreement between two masks in Table 4, these are the percentages of correct and incorrect cloudy and clear classifications of the two masks relative to them

	Cloudy	Cloudy	Clear	Clear
	1st Cloudy	1st Clear	1st Cloudy	1st Clear
	2nd Clear	2nd Cloudy	2nd Clear	2nd Cloudy
MISR ELCM/MODIS operational	54.58	45.42	28.10	71.90
All-R/MISR ELCM	52.07	47.93	44.89	55.11
All-R/MODIS operational	47.98	52.02	17.44	82.56
All-F/MISR ELCM	23.70	76.30	33.36	66.64
All-F/MODIS operational	18.75	81.25	13.04	86.96

scenes and that contained partly cloudy scenes, led to classification accuracies of approximately 94% for the 25 completely clear and overcast scenes.

MODIS radiance (feature) input vectors with expert label training of a QDA classifier produce classification accuracies of 96.43% (95.98%). These results might suggest that MODIS radiance data alone in a QDA classifier might be optimal. However, without scene-by-scene expert labels these accuracies are not possible. Training a QDA classifier on MODIS operational cloud mask results leads to classification accuracies of 89.02% for MODIS radiance input vectors to the QDA classifier and 88.88% for MODIS feature input vectors (Table 3).

The high classification accuracies of those pixels for which the MISR ELCM and MODIS operational masks agreed suggest the possibility of using these pixels as training labels. To test this idea quadratic discriminant analysis classifiers were trained on this subset of pixels on a scene-by-scene basis for the 32 partly cloudy scenes and evaluated against expert labels for the scenes. Overall classification accuracies were 85.23% for MISR radiances, 88.05% for MISR features, 93.62% for MODIS radiances, 93.61% for MODIS features, 93.74% for MISR radiances combined with MODIS radiances, and 93.39% for MISR features combined with MODIS features (Table 3). Scene-by-scene results are illustrated in Fig. 7d–f.

To characterize the relative performances of the MISR ELCM, MODIS operational, and quadratic discriminant analysis classifiers on unlabeled pixels we trained quadratic discriminant analysis classifiers using those pixels for which the MISR ELCM and MODIS operational masks agreed, applied them to the (68%) labeled and (32%) unlabeled pixels in the 32 partly cloudy scenes, and compared the agreement rates of their results with those from the MISR ELCM and MODIS operational cloud mask algorithms (Table 4). In these comparisons we computed the relative tendencies for the algorithms to classify pixels as cloudy or clear. Relative to the expertly labeled pixels, we also computed the percentages of correct and incorrect cloudy and clear classifications of the two masks for those pixels for which they disagreed (Table 5).

4. Discussion

With quadratic discriminant analysis as the classifier, expert labels as training and assessment data and MODIS radiances as the classifier input vectors, a classification accuracy of 96.43% was achieved for the 32 partly cloudy scenes in the study. Using MODIS features as classifier input vectors led to a classification accuracy of 95.98%. With MISR radiances and features as classifier input vectors classification accuracies of 87.51% and 88.45% were achieved (Fig. 7a,b; Table 3). The differences between the MODIS and MISR results are significant at the 99%-level using a *t*-test, indicating that MODIS data have more information for separating clouds from snow- and ice-covered surfaces than MISR data. Combining MISR and MODIS radiances (features) in a quadratic discriminant analysis classifier slightly improved classification rates to 96.98% (96.99%; Fig. 7c, Table 3). The differences between these results and the MODIS- and MISR-only results are significant at the 99%-level using a *t*-test. None of these classification accuracies can be obtained operationally because they rely on the availability of expert labels for all scenes to which they are applied. They do lead to the important observation on how well cloudy and clear pixels are separable in the different feature spaces.

Shi et al. (2004) investigated the performance of classifiers more sophisticated than quadratic discriminant analysis, including a range of support vector machine approaches, but with little improvement in performance relative to quadratic discriminant analysis classifiers. These results suggest that the nonlinear classification boundaries of quadratic discriminant analysis classifiers are sufficiently rich to separate clear and cloudy pixels in daytime polar regions using MISR and MODIS data as feature vectors.

One of the more interesting findings of this study is the classification accuracies (i.e., 96.53% and 99.05%) and scene coverages (i.e., 74.91% and 78.44%) for the partly cloudy and completely clear and overcast scenes of those pixels for which the automated MODIS operational cloud mask and MISR ELCM algorithms were in agreement and for which there were expert labels. Having spectral- and angular-based single-value threshold results in agreement is almost an error free indicator of the class type (i.e., clear or cloudy) for pixels in this study.

This fortuitous result allowed for training a quadratic discriminant analysis classifier scene-by-scene using those pixels in a scene for which the MODIS operational cloud mask and MISR ELCM algorithms agreed. Using the three MISR ELCM features and the six MODIS operational cloud mask features in a quadratic discriminant analysis classifier (i.e., All-F) with training data produced by the two automated algorithms produced a classification accuracy of 93.39% with 100% coverage for the 32 partly cloudy scenes. With the five MISR angular radiances and six MODIS spectral radiances as input to a quadratic discriminant analysis classifier (i.e., All-R) a classification accuracy of 93.74% was attained. These results represent a significant improvement (at the 95%-level of the *t*-test) compared to the single-value threshold results. This improvement is a result of a combination of automatically generated, accurate training data and a flexible and adaptive classifier.

Comparing the relative performances of the MISR ELCM algorithm, the MODIS operational cloud mask algorithm and

the two quadratic discriminant analysis classifiers (Table 4), we found that the agreement rates between cloud mask algorithms were from 3% to 20% lower for the unlabeled, as compared to labeled, pixels. This is not unexpected as the un-labeled pixels contained the cloud edges where classification of pixels is more difficult. The algorithms (i.e., the MISR ELCM algorithm and the QDA classifier with MISR and MODIS features as input vectors, i.e., All-F) using groups of neighboring pixels (i.e., MISR features) as part of their input vectors increased in cloudiness relative to the single pixel algorithms (i.e., the MODIS operational cloud mask algorithm and the QDA classifier with MISR and MODIS radiances as input vectors, i.e., All-R) from the labeled to unlabeled pixels. One possible explanation for this result is that the classifiers using groups of pixels in some of their features tend to classify clear pixels near cloud edges as cloudy ones.

For the labeled pixels the MODIS operational cloud mask algorithm was more likely than the others to classify incorrectly clear pixels as cloudy and the QDA feature-based classifier was more likely to classify incorrectly cloudy pixels as clear (Table 5). Both of these errors contribute to the small percentage (19.62%) of pixels in disagreement labeled as cloudy by the QDA feature-based classifier (i.e., All-F) but clear by the MODIS operational cloud mask. The large increase from labeled to unlabeled pixels of the percentage of pixels classified as cloudy by the QDA feature-based classifier (i.e., All-F) but clear by the MODIS operational cloud mask algorithm (i.e., from 19.62% to 44.95%) is consistent with the interpretation that classifiers with input feature vectors based on groups of pixels are more likely to classify pixels in the vicinity of cloud edges as cloudy than the single pixel classifiers.

The two-class approach adopted for the quadratic discriminant analysis classifier is not appropriate for completely clear and overcast scenes with only one class type. For the 25 completely clear and overcast scenes, though, the MISR ELCM and MODIS operational cloud mask algorithms produced classification accuracies of 95.39% and 93.37% with 100% coverage. These results are comparable to those from the automatically trained quadratic discriminant analysis classifiers for the partly cloudy scenes. An automated algorithm that combines single-value threshold results for completely clear and overcast scenes with quadratic discriminant analysis results for partly cloudy scenes had classification accuracies of approximately 94.5% (Table 6). This represents a significant (at the 95%-level of a *t*-test) improvement over current MISR ELCM and MODIS operational cloud mask algorithm classification accuracies of 91.80% and 91.97%, respectively, for all 57 scenes.

The MODIS and MISR features are relatively stable for clear and cloudy pixels from scene to scene. However, the optimal thresholds that separate clear from cloudy pixels do change from scene to scene and this scene dependence is the source of errors in the single-value threshold classifiers. The high classification accuracies of pixels for which the MODIS operational cloud mask and MISR ELCM algorithms agree demonstrate that tests using both spectral and angular information are filters for incorrect classifications in either of the two approaches alone. Training a QDA classifier scene-by-scene using pixels for which the MODIS operational cloud mask and MISR ELCM algorithms agree produces a classifier with thresholds that are also scene dependent. For such a classifier stability of input feature vectors from scene-to-scene is no longer an issue and one would expect similar results for radiances or features as the input vector elements. As Fig. 7c,f demonstrates, this is the case.

Table 6
Classification accuracies obtained by combining the MISR ELCM algorithm results from completely clear and overcast scenes with the automatic-trained QDA classifier results for partly cloudy scenes

	Number	MISR and QDA-R	MISR and QDA-F
All scenes	57	94.51%	94.43%
Land		94.43%	94.30%
Ocean		94.67%	94.57%

5. Conclusions

In isolation MODIS spectral radiances contained more information for cloud detection than MISR angular radiances. However, the most salient finding in the study was the extremely small classification error rates (3.5% in partly cloudy scenes and 0.9% in completely clear and overcast scenes) when MODIS operational cloud mask and MISR ELCM algorithm results were combined in an automated cloud detection scheme. The relatively large (about 75%) spatial coverage of these combined results permitted automated training of scene-dependent classifiers whose error rate, when applied to all of the pixels in every scene, was about 5%. The information content in MISR and MODIS radiances for operational detection of clouds in daytime polar regions is quite good, with good meaning an error rate less than approximately 5% relative to the expert labels applied to the 57 scenes tested in this study. This is an optimistic assessment. We did not label 32% of the pixels in the 32 partly cloudy scenes because these pixels were often in the vicinity of cloud edges and the expert labels were applied only to unambiguous regions of cloud and clear sky. Our results demonstrated that the rates of agreement between the different cloud masks decreased, relative to the labeled pixels, by 3% to 20% for these unlabeled pixels. We conclude that complicated mixtures of clear and cloudy pixels, such as at cloud edges, will have higher (and difficult to quantify) error rates.

The MISR swath is much smaller than that of MODIS and it takes MISR two days to view all of the Arctic. As this study has demonstrated for a limited data set, MODIS spectral radiances lead to higher cloud classification accuracies than MISR angular radiances. One might then question the value of MISR radiances for cloud detection in polar regions. The value of MISR radiances for cloud detection in daytime polar regions is several-fold. First, this study demonstrated that cloud detection errors from the automated MISR ELCM and MODIS operational cloud mask algorithms occurred for different pixels, hence the error rates of an algorithm based on both are smaller than for the two algorithms separately. Second, MODIS radiance (feature) input vectors, with those pixels for which the MISR ELCM and MODIS operational cloud mask algorithms agreed as training data, for a QDA classifier produced classification accuracies of

93.62% (93.61%) over the 32 partly cloudy scenes. This represents a significant (at the 95%-level of a *t*-test) improvement over the MODIS operational cloud mask algorithm classification accuracies of 90.72%. Third, we found identification of cloudy (but not clear) pixels by the MISR stereo-derived cloud mask algorithm to be extremely reliable, with a classification accuracy of approximately 99%. That is, if the MISR stereo-derived cloud mask classifies a pixel as cloudy, it is cloudy. We did not discuss this result in this paper because the spatial coverage of the MISR stereo-derived cloud mask in the Arctic is quite poor (approximately 26.64%) for the MISR data products that we used.

These findings suggest that MISR data are useful for improving cloud classification accuracies where MISR and MODIS data overlap and that MISR data might be useful in refining cloud detection thresholds applied to MODIS radiances and features from that part of the MODIS swath that does not overlap with the MISR swath. These results also suggest that further analysis of daytime cloud masks obtained from MISR and MODIS radiances over much larger spatial and temporal scales is a worthwhile endeavor. With reasonable cloud mask results, analysis of cloud-top height retrievals from MODIS and MISR will not be dominated by errors in cloud detection. With more reliable cloud detections and cloud-top height assignments in daytime polar regions improvements in the top of atmosphere and surface energy budgets are feasible.

Acknowledgements

Tao Shi and Bin Yu were partially supported by NSF grants CCR-0106656. Bin Yu also benefited from support of an NSF grant DMS-03036508 and ARO grant W911NF-05-1-0104 and a Miller Research Professorship in spring 2004 from the Miller Institute for Basic Research at University of California at Berkeley. For this research Eugene Clothiaux and David Groff were supported by NASA grant NNG04GL93G and Jet Propulsion Laboratory, California Institute of Technology, contract 1259588. Amy Braverman's work is performed at the Jet Propulsion Laboratory, California Institute of Technology, under contract with the National Aeronautics and Space Administration. All MISR data were obtained from the NASA Langley Research Center Atmospheric Science Data Center. All MODIS data were obtained from the NASA Goddard Space Flight Center Earth Sciences Data and Information Services Center. The authors would like to thank Dominic Mazzoni, Larry Di Girolamo, David Diner, Roger Davies, and Ralph Kahn for helpful discussions and suggestions. The reviewers of this paper were extraordinary, providing many, many detailed comments and useful insights. If problems remain in the paper, they are there in spite of the considerable help from the reviewers and are completely our own.

References

Ackerman, S. A., Strabala, K. I., Menzel, W. P., Frey, R. A., Moeller, C. C., & Gumley, L. E. (1998). Discriminating clear sky from clouds with MODIS. *Journal of Geophysical Research*, *103*, 32141−32157.

Ackerman, S., Strabala, K., Menzel, P., Frey, R., Moeller, C., Gumley, L. et al., (2002), Discriminating clear-sky from cloud with MODIS. Algorithm Theoretical Basis Document (MOD35), Version 4, 112 pp.

Di Girolamo, L., & Wilson, M. J. (2000). A first look at band-differenced angular signatures for cloud detection from MISR. *IEEE Transactions on Geoscience and Remote Sensing*, *41*, 1730−1734.

Diner, D. J., Asner, G. P., Davies, R., Knyazikhin, Y., Muller, J. -P., Nolin, A. W., et al. (1999). New directions in Earth observing: Scientific applications of multiangle remote sensing. *Bulletin of the American Meteorological Society*, *80*, 2209−2228.

Diner, D. J., Beckert, J. C., Reilly, T. H., Bruegge, C. J., Conel, J. E., Kahn, R. A., et al. (1998). Multi-angle Imaging SpectroRadiometer (MISR)instrument description and experiment overview. *IEEE Transactions on Geoscience and Remote Sensing*, *36*, 1072−1087.

Jovanovic, V. M., Bull, M. A., Smyth, M. M., & Zong, J. (2002). MISR in-flight camera geometric model calibration and georectification performance. *IEEE Transactions on Geoscience and Remote Sensing*, *40*, 1512−1519.

Jovanovic, V. M., Smyth, M. M., Zong, J., Ando, R., & Bothwell, G. W. (1998). MISR photogrammetric data reduction for geophysical retrievals. *IEEE Transactions on Geoscience and Remote Sensing*, *36*, 1290−1301.

Mardia, K. V., Kent, J. T., & Bibby, S. M. (1979). *Multivariate analysis.* New York: Academic Press.

Muller, J. -P., Mandanayake, A., Moroney, C., Davies, R., Diner, D. J., & Paradise, S. (2002). MISR Stereoscopic image matchers: Techniques and results. *IEEE Transactions on Geoscience and Remote Sensing*, *40*, 1547−1559.

Nolin, A. W., Fetterer, F. M., & Scambos, T. A. (2002). Surface roughness characterizations of sea ice and ice sheets: Case studies with MISR data. *IEEE Transactions on Geoscience and Remote Sensing*, *40*, 1605−1615.

Parol, F., Buriez, J. C., Vanbauce, C., Riedi, J., Labonnote, L. C., Doutriaux-Boucher, M., et al. (2004). Review of capabilities of multi-angle and polarization cloud measurements from POLDER. *Advances in Space Research*, *33*, 1080−1088.

Ripley, B. D. (1996). *Pattern classification and neural networks.* Cambridge University Press.

Rossow, W. B., & Garder, L. C. (1993). Cloud detection using satellite measurements of infrared and visible radiances for ISCCP. *Journal of Climate*, *6*, 2341−2369.

Saunders, R. W., & Kriebel, K. T. (1988). An improved method for detecting clear sky and cloudy radiances from AVHRR data. *International Journal of Remote Sensing*, *9*, 123−150.

Shi, T. (2005), Polar Cloud Detection using Satellite Data with Analysis and Application of Kernel Learning Algorithms. *Doctoral Dissertation, University of California, Berkeley*, pp. 5–56.

Shi, T., Yu, B., Clothiaux, E. E., & Braverman, A. J. (2004). *Cloud detection over snow and ice based on MISR data. Technical Report #663.* University of California at Berkeley: Department of Statistics.

Stephens, G. L., Campbell, G. G., & Vonder Haar, H. T. (1981). Earth radiation budgets. *Journal of Geophysical Research*, *86*, 9739−9760.

Stowe, L. L., Davis, P. A., & McClain, E. P. (1999). Scientific basis and initial evaluation of the CLAVR-1 global clear cloud classification algorithm for the advanced very high resolution radiometer. *Journal of Atmospheric and Oceanic Technology*, *16*, 656−681.

Wielicki, B. A., Barkstrom, B. R., Harrison, E. F., Lee, R. B., Smith, G. L., & Cooper, J. E. (1996). Clouds and the Earth's Radiant Energy System (CERES): An Earth observing system experiment. *Bulletin of the American Meteorological Society*, *77*, 853−868.

Wielicki, B. A., & Green, R. N. (1989). Cloud identification for ERBE radiative flux retrieval. *Journal of Applied Meteorology*, *28*, 1133−1146.

Zavody, A. M., Mutlow, C. T., & Llewellyn-Jones, D. T. (2000). Cloud clearing over the ocean in the processing of data from the Along-Track Scanning Radiometer (ATSR). *Journal of Atmospheric and Oceanic Technology*, *17*, 595−615.